Unusual Size Effects from Tilted Twin Boundaries in Nano-twinned Metals

Sixie Huang[a], I. J. Beyerlein[b], and Caizhi Zhou[a,*]

[a]Department of Materials Science and Engineering, Missouri University of Science and Technology, Rolla, MO 65409, USA

[b]Mechanical Engineering Department, Materials Department, University of California at Santa Barbara, Santa Barbara 93106, USA

ABSTRACT: Tilted twin boundaries (TBs), whose plane normals are rotated at an angle from the parent grain axis, naturally occur in columnar-grained, nano-twinned (NT) metals. Here, using a combination of atomistic simulations and analytical modeling, we reveal that NT metals with the ideal, non-tilted TBs exhibit continuously increasing strength with decreasing twin thickness, and hence, no inverse twin thickness size effect on strength. In contrast, NT metals with tilted TBs exhibit an inverse size effect, and the critical twin thickness, below which strength decreases, increases as the TB-tilt angle increases. The analysis also identifies a critical value of TB tilt, for which strength becomes independent of twin thickness and is the weakest. The transition arises from a change in dislocation activity prevailing mostly on planes inclined to TBs to planes parallel to the TBs. These findings reveal a profound influence of TB tilt angle that could redirect the analysis and engineering of nano-twin structures.

KEYWORDS: Twin boundary, size effect, crystallographic slip model, atomistic simulations

* Corresponding author.

E-mail address: zhouc@mst.edu

1. Introduction

NT metals are polycrystalline metals comprised of micron to submicron sized grains that are nearly completely filled with nanoscale twin lamellae [1, 2]. The twin boundaries (TBs) are coherent and stable against extreme conditions, giving rise to exceptional mechanical properties, such as 5-10 times higher strengths than conventional coarse-grained metals, ductility, and fatigue resistance [1, 3-6]. NT metals also exhibit highly desirable functional properties, such as conductivity [7] and thermal stability [8, 9]. At present, they have become very attractive candidates for the use in high-tech structural applications, next-generation electronic devices and microelectromechanical systems [10, 11]. To further increase their strength, the strategy has been to further reduce the thickness of the twin lamellae. However, a critical twin thickness has been found to exist below which the strength decreases and this strengthening method no longer applies [2].

The origin of the inverse size effect is related to where the dislocations glide and the types of planes on which they glide. Nearly all NTs have an FCC crystal structure, for which there are four types of {111} planes, which are crystallographically equivalent but independently oriented. Also, in an NT, one type of plane lies parallel to the TB, while the other three are inclined to the TB. A positive size effect in strength is expected to originate only for those dislocations that glide inside the lamella (between the TBs) and on one of the three inclined planes. These dislocations are constrained to glide by the two adjacent TBs and hence need to bow out as they thread through the twin lamella. This TB constraint strengthens as the TB spacing or equivalently, the thickness of the lamella λ, decreases, leading to a positive and not an inverse, size effect [12-15]. Dislocations gliding directly on the TBs (and not in-between the TBs) or transmitting from one lamalle, across the TB, to the adjacent lamella are examples of

mechanisms that overcome the TB constraint, and also the former one has been proposed to be responsible for the inverse size effect in strength [13]. Recent tension experiments on single crystal NT Cu pillars have demonstrated that twin boundary migration in *tilted twin boundaries* can also lead reduced strengths in NTs. In the idealized NT, the grains are columnar, and the TBs span the grain cross-section, lying normal to the long axis of the columnar grain (see Fig. 1(c)). Tilted TBs have their TB rotated from this ideal TB orientation, by 10° to 45° [17]. Most NTs have some fraction of their TBs tilted (e.g., see Figures 1(a), (b)) [18-19].

Despite its prevalence in many NT metals, the effect of the TB-tilt angle with respect to the loading direction on the size scaling on strength has not been addressed. Here we perform molecular dynamics (MD) simulations to study the effect of TB orientation on the strength and deformation mechanisms in columnar-grained NT metals.

2. Methodology

Materials fabricated by deposition techniques typically have a columnar structure with small aspect ratios and tilted TBs with the tilt angles θ, ranging from about 10° to 45° (where θ is defined in Figure 1(d)). The variation in tilt depends on the material and parameters used in deposition [18-20]. Figure 1(a) and (b) show the finely twinned microstructures for NT Ag and NT Cu. In NT Ag, the range of TB tilt angles is approximately 10°~15° [18], while for NT Cu the range is broader spanning 10°, 15° and 45° [19]). In the plane of the layer the shape of the grains is approximately hexagonal.

MD simulation is used to determine the effect of tilted twin boundaries on size effects in NT. This method is well suited for taking into account both the resolved shear stress and explicit microstructure features, such as TB tilt angle θ, grain size, and twin thickness λ on where and

when dislocations glide. Figure 1 (c)-(e) show the MD model of columnar-grained NT structures in present simulations. In this model, the grains in the starting NT microstructure have a hexagonal shape cross-section in plane and a thickness equal to that of the layer. Periodic boundary conditions are imposed along all three directions. Lengths in the X and Y directions vary with grain size D and the length in the Z direction varies with the twin plane tilt angle θ and twin thickness λ (as defined in Figure 1(d)). The tensile direction corresponds to the Z direction. We varied θ, from 0° to 60° with respect to the XY-plane and λ from 0.6 nm - 3.7 nm with two different grain sizes, D: 10 nm and 20 nm. To create stable, high-angle tilt grain boundaries between each grain, grains B-D were rotated by 30°, 60° and 90° relative to grain A, as shown in Figure 1(e). To tilt the TBs, the grains were rotated to the desired angle θ relative to the original [110] direction.

The MD simulations were performed using the LAMMPS code [21] with embedded-atom method (EAM) potentials for Cu [22], Ag [23], and Au [24]. The conjugated gradient method was used to first relax the system and then the samples were equilibrated in Nose/Hoover isobaric-isothermal ensemble (NPT) for 100 ps with 300 K. After relaxation, uniaxial tension was applied on the sample with a constant strain rate of 1×10^{8} s^{-1}. This strain rate is much higher than those used in actual experimental tests but are characteristic of this type of simulation method [25]. In particular the rate employed here is commonly used in MD simulations of NT metals [13, 15, 17].

OVITO was used to visualize the configuration of atoms in the microstructure [26]. With this information, we can determine on which planes and where dislocations glide, making the important distinctions between TB-parallel glide (on planes parallel to the TB and inside the

twins), TB-inclined glide (on planes parallel to the TB and inside the twins), and TB-glide (directly on the TBs).

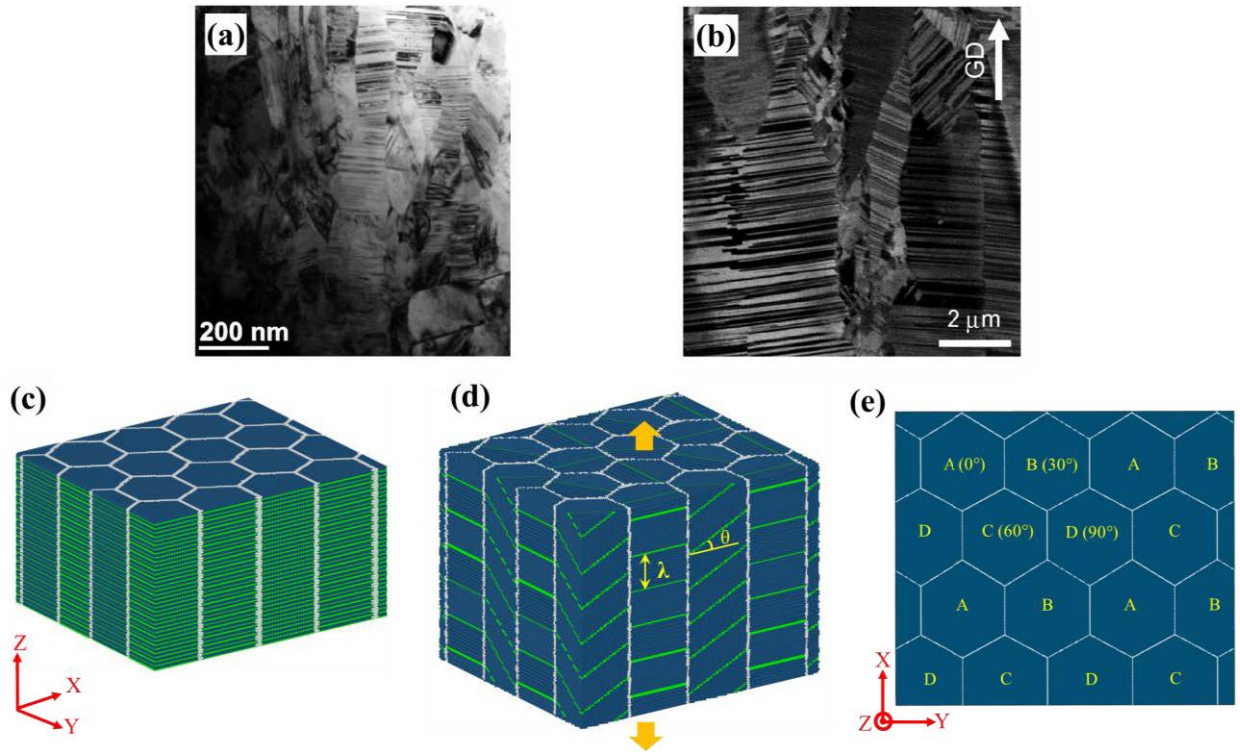

Figure 1. Microstructures of NT structures prepared by electrodepositions with tilted twin boundaries: (a) columnar grained Ag [18] and (b) columnar grained Cu [19] with the marked growth direction (GD). Initial structures used in simulations with (c) λ = 0.6 nm and θ = 0°, (d) λ = 3.7 nm and θ = 43° (e) View from z direction in (c). X-[110], Y-[$\bar{1}1\bar{2}$] and Z-[$\bar{1}11$] for grain A, grains B-D are rotated along Z axis with specific angle. Atoms in all figures are colored using the Common Neighbor Analysis (CNA). FCC, HCP and unknown atoms are blue, purple and white, respectively)

Further, to evaluate the amounts of plastic deformation induced by partial or full dislocation glide, we employed the atomic-shift analysis developed by Vo et al. [27]. From these atomic shifts, the total amount of strain contributed by partial or full dislocation glide at any

point in the deformation can be calculated by summing the strain induced by all N atoms displaced by dislocation motion, as follows:

$$\varepsilon^{dis} = \sum_i^N \frac{A}{V}(\bar{l} \cdot \bar{b}_i)(\bar{l} \cdot \bar{n}_i) \quad (1)$$

where $\bar{b}_i$ is the Burgers vector of the dislocation slipping over the atom i, $\bar{n}_i$ is the unit normal of the slip plane for the dislocation slipping over the atom i, $\bar{l}$ is the loading direction, A is the unit area of atoms projected on the slip plane, V is the volume of the simulation box, and N is the total number of slipped atom.

3. Results

Figure 2 (a) and (b) show the stress-strain curves for the NT Cu samples with different TB θ. In efforts to study a representative measure of NT strength, we averaged the computed stresses within a strain range of 7–15%, as is done in similar atomistic modeling work [13, 28]. Figure 2 (c) plots the average flow stress versus twin thickness λ for all tilt angles. First, it is found that θ has a profound effect on the size scaling in strength, and even more significantly, some TB θ exhibit little to no size effect in strength.

For reference, we first consider the ideal $\theta = 0°$ TB orientation, which corresponds to the conventionally studied representation for epitaxially grown NT nanostructures. For this case, the strengthening effect is continuous and no "softening" (or an inverse size effect) is observed even as λ is reduced to the finest nanoscale thickness of 0.6 nm. This result indicates excellent mechanical and microstructural stability and is consistent with prior experimental studies that shows sputtered highly textured NT Cu does not have softening [29].

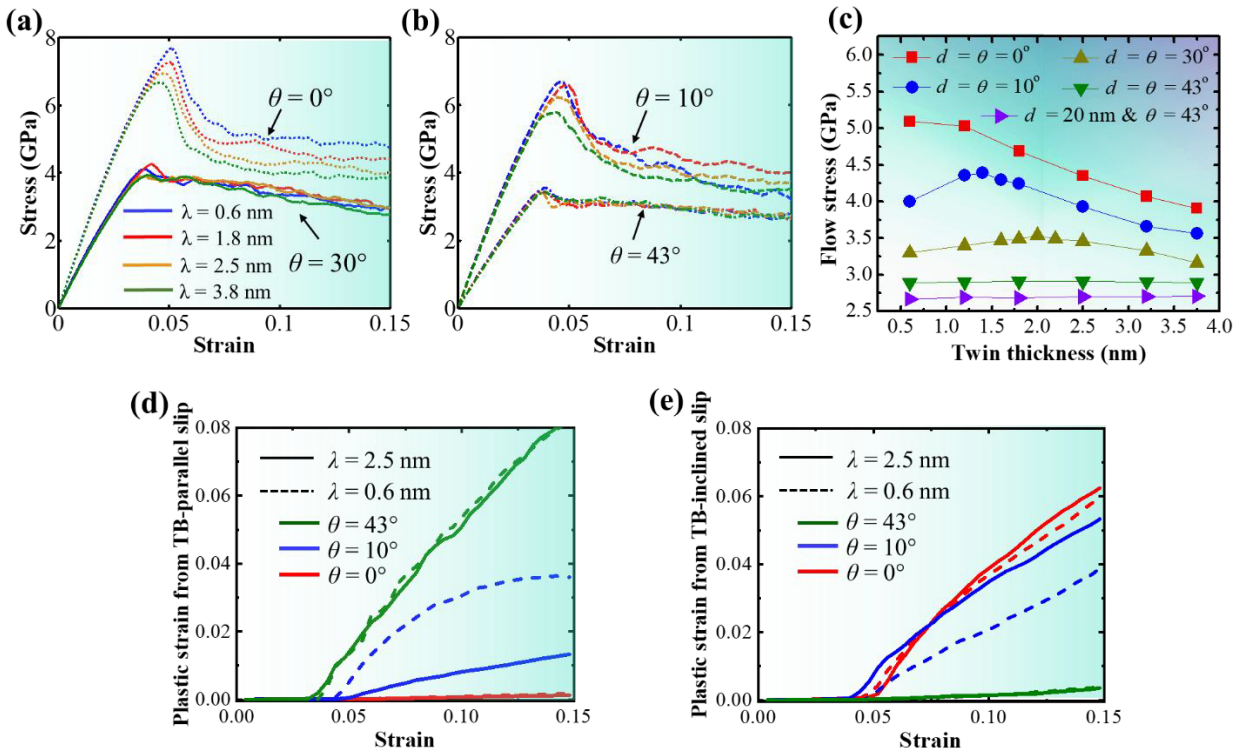

Figure 2. Stress-strain curves for samples with D = 10 nm (a) θ = 0° and 30°; (b) θ = 10° and 43°. (c) Plot of the average flow stress versus the twin thickness for NT Cu samples with d = 10nm and 20nm. Plastic strain from TB-parallel (d) and TB-inclined (e) slips for λ = 0.6 and 2.5 nm.

To identify the deformation mechanisms, we employed the atomic-shift analysis developed by Vo et al. [27], to evaluate the amounts of plastic deformation induced dislocation glide. Atomic-shift analysis in Figure 2 (d-e) indicates that, for the full range of λ, dislocations glide on the slip planes inclined to the TB. Therefore, they must be threading through the layers, inside the twin lamellae. Theoretically, the stress to propagate the dislocation by threading, or confined layer slip (CLS), increases as $\ln(h')/h'$, were $h' = h/b$ is normalized by the value of the Burgers vector [30, 31]. This mode of dislocation propagation would become increasingly constrained and difficult as λ decreases and is fully consistent with the observed strengthening in the NT as λ decreases. When λ drops below 1.0 nm, on the order of a dislocation core size,

multiple, necklace-like extended dislocations, containing jogs bounded by neighboring twin planes, appear during the deformation (Supporting Information, Figure S1). These extended jogged dislocations were also observed in recent atomistic simulations and experiment studies in NT Cu with various layer thicknesses [15, 32]. The critical stress to activate these jogged dislocations is approximately 7.7 GPa and 7.3 GPa for λ = 0.6 nm and 0.8 nm in our samples and proportional to $1/\lambda$ [15]. None of these mechanisms would lead to degradation in strength, as λ decreases to the atomic-scale, explaining why the NT continues to strengthen as λ drops to even below 1.0 nm.

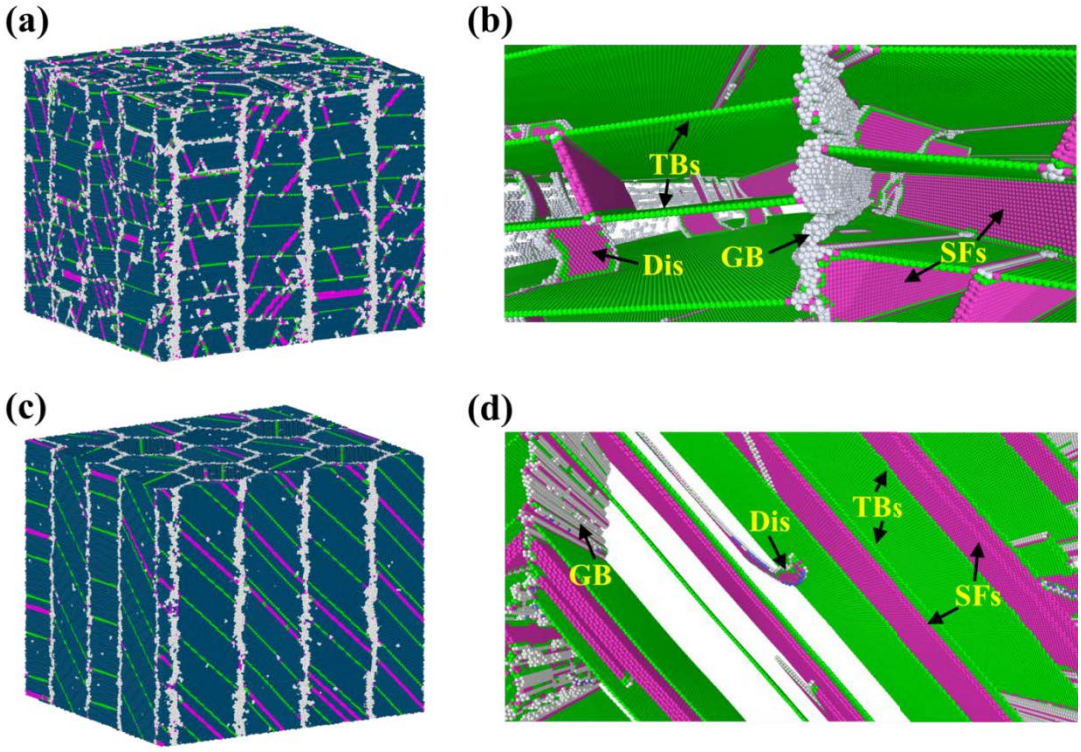

Figure 3. Microstructures of 7% strain deformed sample with λ = 3.7 nm and D = 10 nm, (a) and (b) for θ = 10°. (c) and (d) TB for θ = 43°. Atoms in twin boundary are colored green. FCC Atoms are set invisible in (b) and (d).

For cases with tilted twin boundaries ranging from θ = 10º to 30º, an inverse size effect regime manifests. The strength increases as λ decreases up to a critical thickness λ_c, and then as λ decreases further below λ_c, the strength decreases. For $\lambda > \lambda_c$, multiple stacking faults intersecting twin boundaries are observed, suggesting that the dislocations glide on inclined planes (Figure 3(a) and (b)). The critical λ_c is seen to depend on TB-tilt θ. For θ =10º, λ_c = 1.4 nm and for θ = 30º, λ_c = 2.2 nm. Figure 2(d-e) presents results from the atomic-shift analysis indicating that dislocation glide occurs predominantly on the TB-inclined glide planes for $\lambda > \lambda_c$, but via a combination of TB-parallel and TB-inclined slip for $\lambda < \lambda_c$. Thus, the critical λ_c that marks the transition from strengthening to softening corresponds to a change from exclusive inclined slip to a combination of TB-inclined and TB-parallel slip. As TB-tilt increases, this transition occurs at a higher critical λ_c.

For θ = 43º, an interesting two-step microstructural evolution was observed. First, the TB angle reorients in elastic deformation, until it increases to 45°, and next, the material begins to deform plastically. After achieving this step, the stress-strain responses in the second step are similar for the entire range of λ (Figure 2 (b)).

This result is different than the inverse-size-effect regime seen in the microstructures with θ =10º and 30º, since the strength in the softening regime is by definition still affected by λ, albeit decreasing with λ. An atomic-shift analysis is carried out for this range (43˚$\pm$2˚) and the results are shown in Figure 2 (d-e). It is identified that all dislocations glide on slip planes lying parallel to the TBs. The glide of these dislocations is not constrained by the TBs, and hence, why twin thickness λ has no effect on strength for θ = 43˚$\pm$2˚.

Calculations performed here identify a strong effect of NT TB tilt on the NT size scaling in strength. To the best of our knowledge, although NTs materials naturally contain tilted twin boundaries, this phenomenon has not been evaluated experimentally, and thereby motivates further considerations of twin boundary tilt effects, in addition to the usual layer thickness effects. We note that the strengths calculated here are obtained from atomistic calculations using applied strain rates that significantly higher than those normally used in NT experimental testing [19]. These high levels of strain rate, however, are common for atomistic simulation and in fact the rates employed here are similar to those also applied in previous MD simulation studies on NT Cu [13, 15]. Despite the large discrepancy in rates, MD simulations have proven successful in revealing underlying deformation mechanisms in NT metals also seen in experiments. For instance, by using the same loading method in their MD simulations, Li et al. have identified that the twin-boundary migration results from nucleation and motion of partial dislocations on the twin planes [13]. Likewise, Zhou et al. revealed that the extended jogged dislocations formed in a columnar-grained nanotwinned metal subjecting to an external stress parallel to the twin planes [15]. It is shown here that the origin of these size effects and TB orientation effects are based on dislocation nucleation, motion, and crystallography. Since these same features are known to dominate at lower rates, the trends reported here ought to prevail at lower rates.

4. Discussion

4.1 GB Analysis

In previous studies [13], the inverse size effect in NT Cu was attributed to the nucleation and glide of dislocations on the TBs. It was rationalized that samples with smaller twin thicknesses carry a higher density of grain-boundary/twin intersections with high stress concentrations,

resulting in more available sources gliding for dislocations to glide on the TBs and not in between them.

To quantitatively analyze the effect of λ on the stress concentration on the GB atoms in the case in which slip predominantly occurs on parallel slip planes, we calculate the stress distributions for the six stress components and the resolved shear stress (RSS) on the GB atoms for two 43° samples with λ = 0.6 and 2.5 nm, both of which have the same simulation box size (See Figure S5). Based on the stress distributions in Figure S5 (a)-(g), these two samples developed similar GB atom stress distributions. Since there is no difference on the GB atom stresses between the twin boundary spacing λ = 0.6 and 2.5 nm, TB-glide cannot explain the thickness-independent strength for 43º samples observed here.

Since in an FCC material, the TB coincides with a slip plane, an important distinction to be made is whether dislocations glide inside the twin lamella, between the TBs, or directly on the TBs. As mentioned, the basic assumption in the earlier explanations is that all dislocations on the parallel slip planes can only nucleate and glide on the twin boundaries [13]. Figures 3(b) and 3(d) from the present simulations find that while some dislocations nucleate and glide on the TBs, a large number of dislocations nucleate and glide on TB-parallel slip planes within the twin lamella. Furthermore, those dislocations that glide on the TBs cause the TB to migrate and enlarge the twin. Once the lamella has thickened, dislocations proceed to glide on planes inside them and TB-inclined slip becomes favorable. Therefore, TB-glide is not predominant and not sustained for most of the deformation and cannot explain the observed inverse size effect.

4.2 Thickness-Independent Strength

In addition to mechanical stress, *microstructural* features, such as twin thickness and TB-tilt angles, also affect which slip systems are activated and the rates of plastic slip on these systems, within mechanically strained NTs. In the MD calculations of NT response, two modes of slip are identified via analysis of the atomic shifts in the GB, TBs, and twin lamellae: TB-inclined and TB-parallel slip, classified by the orientation relationship of their planes with the TBs. In what follows, to explain the observed unusual size effects on strength, the relationships between microstructure and the rates of slip via these two modes, as governed by the RSS on these systems, are analyzed. Following Orowan's kinematic equation for dislocations, the relationship between the total plastic strain rate and dislocation slip rates within the twin lamella of the NT is given by

$$\dot{\varepsilon}_{tot} = \frac{1}{M_I}\dot{\gamma}_I + \frac{1}{M_P}\dot{\gamma}_P \quad (1)$$

The first and second terms in Eq. (1) represent the plastic strain contribution from the TB-inclined and the TB-parallel slip systems, respectively, and M_I and M_T are the Taylor factors for the TB-inclined and TB-parallel slip systems, which reflect the highest Schmid factors of these systems. To formulate $\dot{\gamma}_I$ and $\dot{\gamma}_P$, the maximum amount of slip possible for a given twin thickness and slip plane is assumed. Physically, this implies that dislocations nucleated at one boundary are able to glide unhindered across the grain and annihilate at the opposing boundary. In this event, for TB-inclined slip, the amount of slip provided by every dislocation emitted from the boundary is given by $\frac{b}{D}$. The dislocation must thread through an individual twin lamella, resisted by a critical stress τ_{CLS}, representing the pinning effect of the flanking TBs spaced λ apart [33]. In contrast, for TB-parallel slip, the full extent of glide would be limited by the grain size D, and consequently, the amount of slip induced by each TB-parallel event is $\frac{\lambda}{b}$. The

threshold stress τ_P to activate TB-parallel slip is given by the critical stress to nucleate dislocations from the GBs [34]. The shear strain rates on inclined slip, $\dot{\gamma}_I$, and parallel slip, $\dot{\gamma}_P$, are estimated using transition state theory, which is appropriate when dislocation glide is controlled by thermal activation. On this basis, in the Supporting Information Note 3, the following rate expressions are derived for $\dot{\gamma}_I$, and $\dot{\gamma}_P$,

$$\begin{cases} \dot{\gamma}_I = k_I \frac{\lambda}{b} \nu_D \, exp\left(-\frac{Q-(\tau^I_{RSS}-\tau_{CLS})\, V^*_I}{RT}\right) \\ \dot{\gamma}_P = k_P \frac{D}{b} \nu_D \exp(-\frac{Q-(\tau^P_{RSS}-\tau_P)V^*_P}{RT}) \end{cases} \quad (2)$$

where ν_D is the Debye frequency, b is the Burgers vector, k_I and k_P are the activation efficiency constants, τ^I_{RSS} and τ^P_{RSS} are the resolved shear stress, V^*_I is the activation volume for inclined slip and V^*_P is the activation volume for parallel slip, Q is the activation energy for dislocation glide [34]. (Values used for Cu for the calculations below are given in the supplement.) Note that the key differences in the rates of these two modes manifest in the pre-factor and required thermal energy for glide, which arise from the way microstructure has distinguished the amounts of slip each provides and the resistances to glide they encounter. Consistent with the assumption that the grain boundaries are perfect sinks, these expressions do not include the development of (anisotropic) back stresses during deformation. Since all dislocations reaching the boundary are annihilated, dislocations are not stored within the grains and back stresses are not generated.

The expressions for these two slip rates in Eqns. (2) highlight a key difference: the inclined shear strain rate is twin-thickness dependent but grain-size independent, while the parallel shear strain rate is twin-thickness independent but grain-size dependent. Therefore, when the plastic strain rate is predominantly contributed from the TB-parallel slip systems, the flow

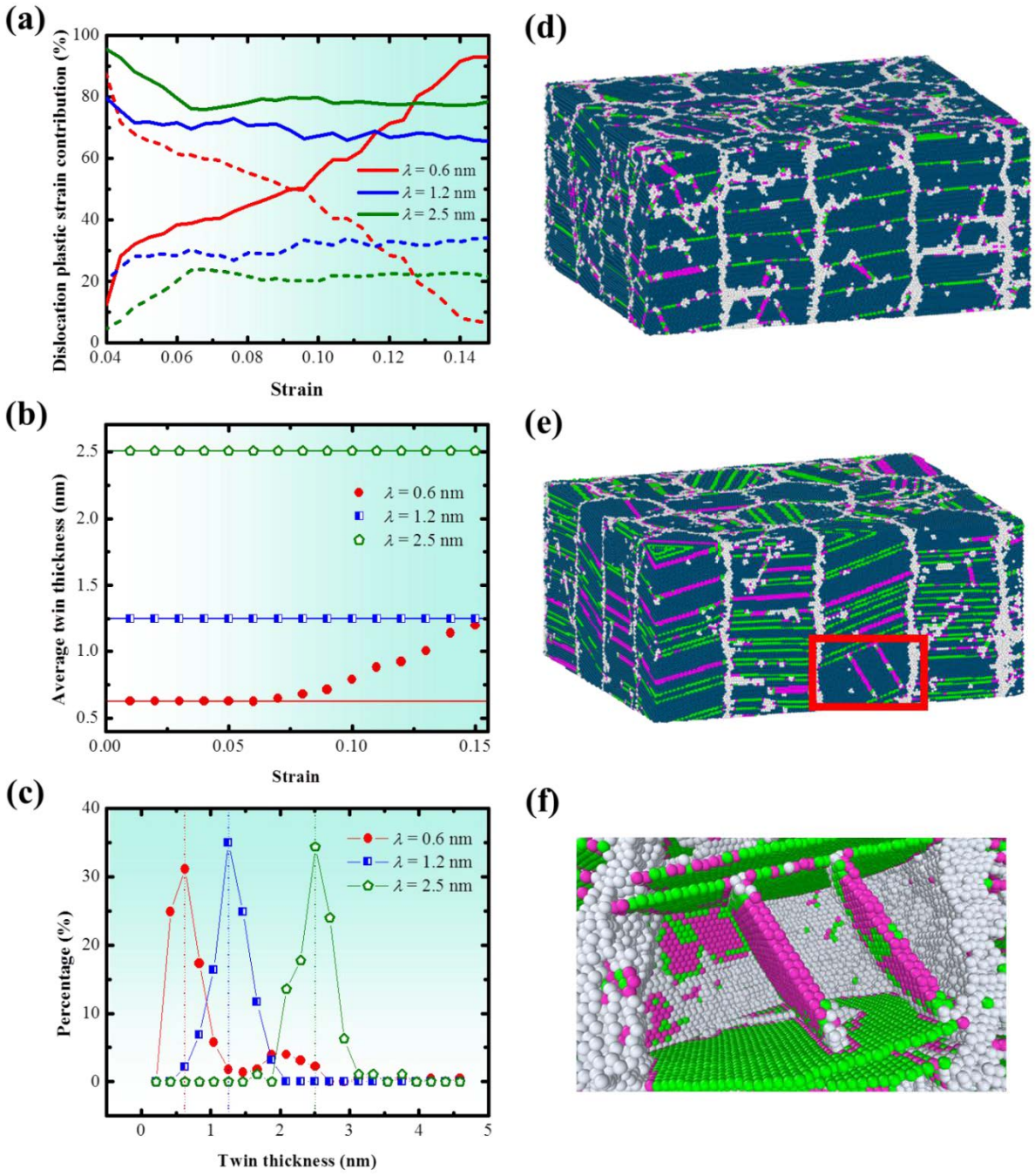

Figure 4. (a) Evolution of the plastic strain contributions after yielding for NT Cu with $\theta = 10°$. Solid and dashed lines are for inclined and parallel slips, respectively. (b) Evolution of the average twin thickness versus strain. (c) Distributions of twin thicknesses at 12% strain (Vertical lines indicate the initial twin thicknesses for each case). Microstructures of deformed samples at 12 % strain: (d) $\lambda = 2.5$ nm, (e) $\lambda = 0.6$ nm, (f) a local thicker twin region in (e).

stress becomes twin thickness independent. This explains why the average flow stress, as shown in Figure 2 (c), is thickness independent for $\theta = 43^{\circ}$.

4.3 Origin of the Inverse Size Effect

Based on the present simulation results, the softening effect is caused by dislocation activity on both TB-parallel and inclined slip planes, not only TB-parallel glide as is commonly thought. Figure 4 (a) illustrates the effect of twin thicknesses on plastic strain contributions from dislocations gliding on TB-inclined and TB-parallel slip systems for a TB-tilt of $\theta = 10°$. Dislocations gliding on TB-inclined slip planes are seen to accommodate a majority of the strain for samples with λ = 1.2 nm and 2.5 nm. Only for samples with very fine λ = 0.6 nm does TB-parallel glide dominate the early stages of plastic deformation. However, as the applied strain increases, the contribution from TB-inclined dislocation glide continuously increases and eventually exceeds that from TB-parallel glide.

When dislocations glide on the TB boundary, they cause the boundary to migrate. Changes in twin thickness with strain were analyzed to determine whether TB boundary migration occurred. Figure 4(b) shows the results from this analysis for the case of TB-tilt of $\theta = 10°$. When the original thickness λ is greater than the λ_c , e.g., λ =1.2 nm and 2.5 nm, the twin thickness is the same before and after deformation, as shown in Figure 4 (d). For the sample with λ smaller than the λ_c , e.g., λ = 0.6 nm, when the material softens, the average twin thickness is seen to increase with the strain. Further analysis in Figure 4(e) finds that the dislocation glide activity on the TBs at the beginning of the plastic deformation results in TB migration and subsequent annihilation, leaving larger twin lamellae than before. For instance, the distributions of twin thickness at 12% strain in Figure 4(c) indicate that more than 10% twin lamellae in the λ

= 0.6 nm sample possess twin thicknesses larger than 2.0 nm. After the twin thickness has widen in the early stages of straining, TB-inclined slip activity is encouraged and increases in relative amounts as strain increases. Therefore, the inverse size effect is a consequence of TB-inclined dislocation slip within enlarged twin laminae (Figure 4(f)), larger than the initial λ. In addition, our study has revealed that the twin boundary migration induced by the dislocation gliding on the TBs can result in detwinning, as shown in Figure 4(e). As mentioned earlier, the simple crystallographic slip model, found in the Supporting Information, indicates that the critical stress to activate dislocation gliding on the TBs is affected by the grain size, with smaller grain sizes leading to higher critical stresses. Accordingly, detwinning would also be affected by the grain size. It is not surprising that experimental studies [14] reported considerable detwinning when twin spacing, λ, is several nanometers thick, since the grain size in actual samples is much larger than the grain size of 10 nm used in our study. Furthermore, we found the probability of detwinning process decreases with the increase of λ. Although we observed detwinning in our simulations with λ at 1.0-2.0 nm, the total amount of detwinning activity is much lower than that in the sample with $\lambda = 0.6$ nm.

A previous study by Li et al [13] reported that the critical twin spacing for softening is affected by the grain size: the smaller the grain size, the smaller is the critical twin-boundary spacing. In the experimental studies by Lu el al [2] the critical spacing of $\lambda < 15$ nm was reported for material with a large grain size, in the range of 400 to 600 nm. The grain size in this study was much smaller, at 10 nm, due to computational time efficiency, and therefore, the critical twin spacing found here would also be much smaller than observed experimentally. The very fine twin layer thicknesses in the NTs considered here (0.6 nm to 3.7 nm) have been studied experimentally [35], but yet they are still relatively finer compared to most NT samples studied

to date (e.g., 5 nm to 100 nm) [19]. As long as deformation in samples with larger twin thicknesses is dominated by crystallographic slip in the layers then the conclusions made here ought to still apply.

4.4 Generalized Deformation Map for NT Metals

Combining our results with findings from previous works, Figure 5 maps the regimes for the predominant deformation mechanisms on a plot with axes of the normalized strength and twin thicknesses. Results from this work provide several important components in the bottom region and middle region on this map. The bottom region narrowly encompasses those tilts centered about 43°. Deformation involves predominant TB-parallel slip, which does not incur a size effect. The bottom region narrowly encompasses those tilts centered about 43°. Deformation involves predominant TB-parallel slip, which does not incur a size effect. In the top region with the highest strength and TB angles very close to 0º, plastic deformation is dominated by TB-inclined slip, which gives rise to a strong, positive size effect. The middle region includes all other TB-tilt angles, in which slip activities on both TB-inclined and TB-parallel planes can be activated. The inverse size effect is induced by the transition from TB-parallel to TB-inclined slips as "Mixed Parallel/CLS slip" in Figure 5. For cases with large λ, Frank-Read (FR) sources can generate the plastic strain that can induce dislocation pile-ups near the TBs.

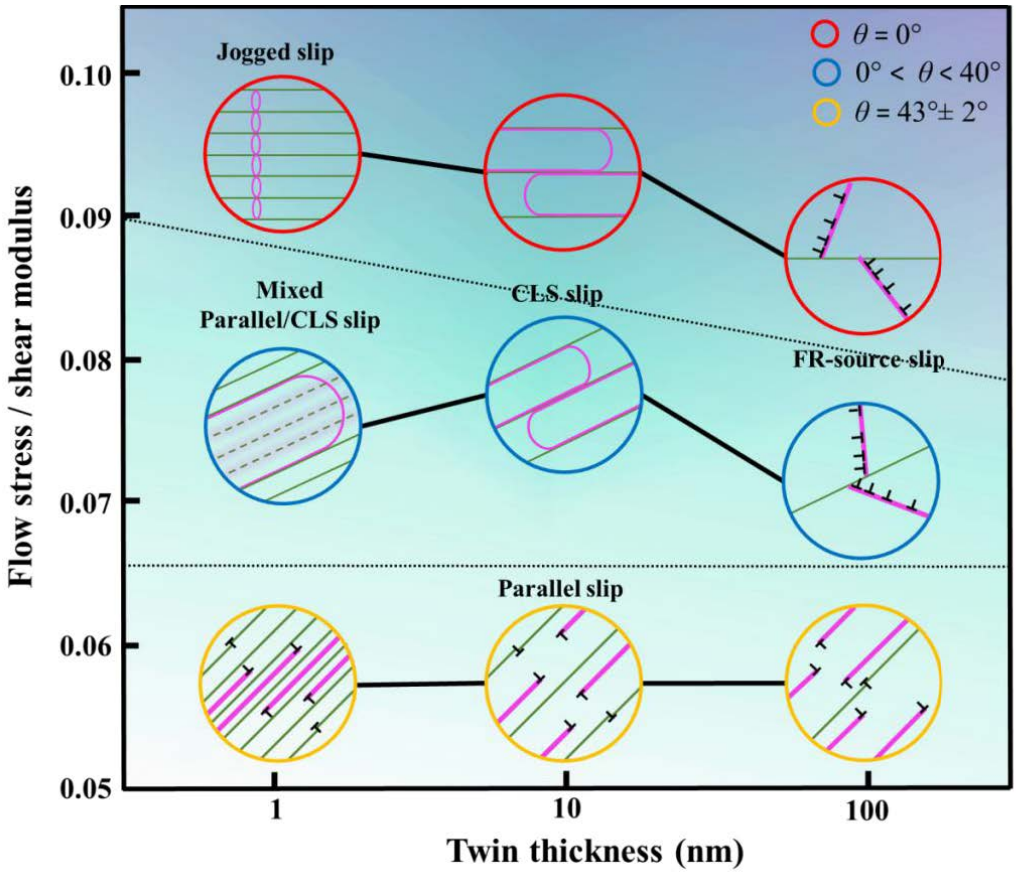

Figure 5. Generalized deformation map for NT metals as a joint function of twin boundary spacing and strength.

5. Conclusions

In summary, using atomistic simulation, we investigate the effects of twin boundary (TB) tilt on the twin-layer size effects on strength. The analysis reveals links between TB-tilt, slip activity, and macroscopic stress-strain curves. While the effects of tilt for some common cases, such as for 0° and 45° tilts, may be intuitive, many interesting, unexpected behaviors arise for intermediate tilt angles. It reveals that the inverse size effect in strength of NT metals is induced by changes in dislocation activity from gliding on planes inclined to the TBs to planes parallel to the TBs. Only in the case of ideal 0° tilt, is this size effect induced softening not predicted. This

work also identifies the critical range of values of TB tilt for which the strength of the NT metals becomes insensitive to twin thickness. These findings shed light on the role of dislocation mechanisms in the plasticity of NT FCC metals and can benefit he design and processing of ultrahigh strength ductile NT metals.

Acknowledgements

This work was supported by NSF CAREER Award (CMMI-1652662). I.J.B acknowledges support by the U.S. DOE, Office of Basic Energy Sciences Program DE-SC0018901. The supercomputer time allocation was provided by XSEDE (DMR170093).

References

[1] Lu L, Shen Y, Chen X, Qian L, Lu K. Ultrahigh strength and high electrical conductivity in copper. Science 2004;304:422.
[2] Lu L, Chen X, Huang X, Lu K. Revealing the maximum strength in nanotwinned copper. Science 2009;323:607.
[3] Ma E, Wang Y, Lu Q, Sui M, Lu L, Lu K. Strain hardening and large tensile elongation in ultrahigh-strength nano-twinned copper. Applied Physics Letters 2004;85:4932.
[4] Beyerlein IJ, Zhang X, Misra A. Growth twins and deformation twins in metals. Annual Review of Materials Research 2014;44:329.
[5] Li X, Dao M, Eberl C, Hodge AM, Gao H. Fracture, fatigue, and creep of nanotwinned metals. MRS Bulletin 2016;41:298.
[6] Wang J, Zhang X. Twinning effects on strength and plasticity of metallic materials. Mrs Bulletin 2016;41:274.
[7] Chen X, Lu L, Lu K. Electrical resistivity of ultrafine-grained copper with nanoscale growth twins. Journal of Applied Physics 2007;102:083708.
[8] Anderoglu O, Misra A, Wang H, Zhang X. Thermal stability of sputtered Cu films with nanoscale growth twins. Journal of Applied Physics 2008;103:094322.
[9] Bufford D, Wang H, Zhang X. Thermal stability of twins and strengthening mechanisms in differently oriented epitaxial nanotwinned Ag films. Journal of Materials Research 2013;28:1729.
[10] Zhu YT, Liao X. Nanostructured metals: retaining ductility. Nature materials 2004;3:351.
[11] Pan Q, Zhou H, Lu Q, Gao H, Lu L. History-independent cyclic response of nanotwinned metals. Nature 2017;551:214.
[12] Zhu T, Li J, Samanta A, Kim HG, Suresh S. Interfacial plasticity governs strain rate sensitivity and ductility in nanostructured metals. Proceedings of the National Academy of Sciences 2007;104:3031.
[13] Li X, Wei Y, Lu L, Lu K, Gao H. Dislocation nucleation governed softening and maximum strength in nano-twinned metals. Nature 2010;464:877.
[14] Li N, Wang J, Zhang X, Misra A. In-situ TEM study of dislocation-twin boundaries interaction in nanotwinned Cu films. Jom 2011;63:62.
[15] Zhou H, Li X, Qu S, Yang W, Gao H. A jogged dislocation governed strengthening mechanism in nanotwinned metals. Nano letters 2014;14:5075.
[16] Wang J, Li N, Anderoglu O, Zhang X, Misra A, Huang J, Hirth J. Detwinning mechanisms for growth twins in face-centered cubic metals. Acta Materialia 2010;58:2262.
[17] Jang D, Li X, Gao H, Greer JR. Deformation mechanisms in nanotwinned metal nanopillars. Nature nanotechnology 2012;7:594.
[18] Ott R, Geng J, Besser M, Kramer M, Wang Y, Park E, LeSar R, King A. Optimization of strength and ductility in nanotwinned ultra-fine grained Ag: Twin density and grain orientations. Acta Materialia 2015;96:378.
[19] You Z, Lu L, Lu K. Tensile behavior of columnar grained Cu with preferentially oriented nanoscale twins. Acta Materialia 2011;59:6927.
[20] Brons J, Padilla Ii H, Thompson G, Boyce B. Cryogenic indentation-induced grain growth in nanotwinned copper. Scripta Materialia 2013;68:781.
[21] Plimpton S. Fast parallel algorithms for short-range molecular dynamics. Journal of computational physics 1995;117:1.

[22] Mendelev M, Kramer M, Becker CA, Asta M. Analysis of semi-empirical interatomic potentials appropriate for simulation of crystalline and liquid Al and Cu. Philosophical Magazine 2008;88:1723.
[23] Williams P, Mishin Y, Hamilton J. An embedded-atom potential for the Cu–Ag system. Modelling and Simulation in Materials Science and Engineering 2006;14:817.
[24] Ackland G, Tichy G, Vitek V, Finnis M. Simple N-body potentials for the noble metals and nickel. Philosophical Magazine A 1987;56:735.
[25] Bulatov V, Cai W. Computer Simulations of Dislocations. Oxford University Press 2013.
[26] Stukowski A. Visualization and analysis of atomistic simulation data with OVITO–the Open Visualization Tool. Modelling and Simulation in Materials Science and Engineering 2009;18:015012.
[27] Vo N, Averback R, Bellon P, Odunuga S, Caro A. Quantitative description of plastic deformation in nanocrystalline Cu: Dislocation glide versus grain boundary sliding. Physical Review B 2008;77:134108.
[28] Schiøtz J, Jacobsen KW. A Maximum in the Strength of Nanocrystalline Copper. Science 2003;301:1357.
[29] Zhang X, Misra A. Superior thermal stability of coherent twin boundaries in nanotwinned metals. Scripta Materialia 2012;66:860.
[30] Feng X, Hirth J. Critical layer thicknesses for inclined dislocation stability in multilayer structures. Journal of applied physics 1992;72:1386.
[31] Embury JD, Hirth JP. On dislocation storage and the mechanical response of fine scale microstructures. Acta Metallurgica et Materialia 1994;42:2051.
[32] Lu Q, You Z, Huang X, Hansen N, Lu L. Dependence of dislocation structure on orientation and slip systems in highly oriented nanotwinned Cu. Acta Materialia 2017;127:85.
[33] Misra A, Hirth J, Hoagland R. Length-scale-dependent deformation mechanisms in incoherent metallic multilayered composites. Acta materialia 2005;53:4817.
[34] Zhu Y, Liao X, Srinivasan S, Zhao Y, Baskes M, Zhou F, Lavernia E. Nucleation and growth of deformation twins in nanocrystalline aluminum. Applied physics letters 2004;85:5049.
[35] Cheng Z, Zhou H, Lu Q, Gao H, Lu L. Extra strengthening and work hardening in gradient nanotwinned metals. Science 2018;362:eaau1925.

Supporting Information for

"Unusual Size Effects from Tilted Twin Boundaries in Nano-twinned Metals"

Sixie Huang[a], Irene. J. Beyerlein[b] , and Caizhi Zhou[a]

[a]Department of Materials Science and Engineering, Missouri University of Science and Technology, Rolla, MO 65409, USA

[b]Mechanical Engineering Department, Materials Department, University of California at Santa Barbara, Santa Barbara 93106, USA

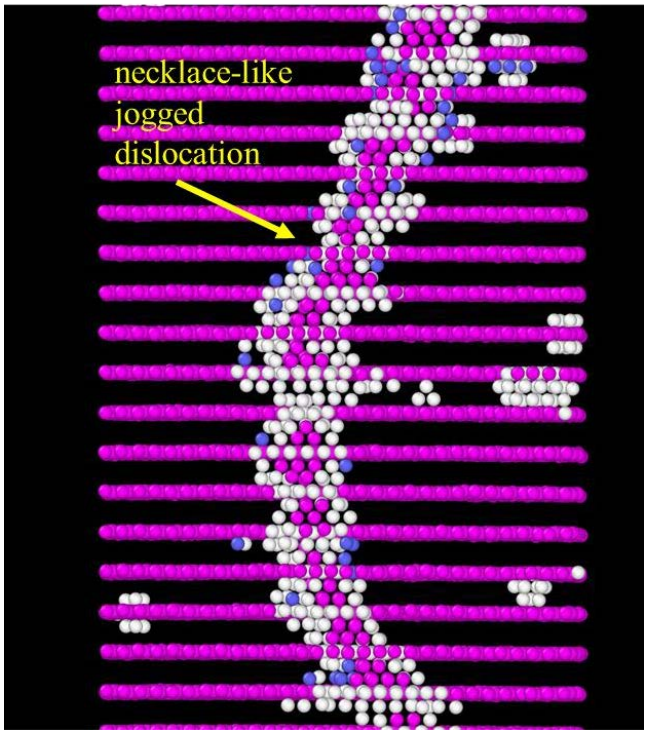

Figure S1. Microstructure of the NT Cu sample with $\theta = 0°$, $D = 10$ nm and $\lambda = 0.6$ nm at 10% strain. Glide of necklace-liked jogged dislocation is observed in this structure. GB atoms have been hidden in this microstructure.

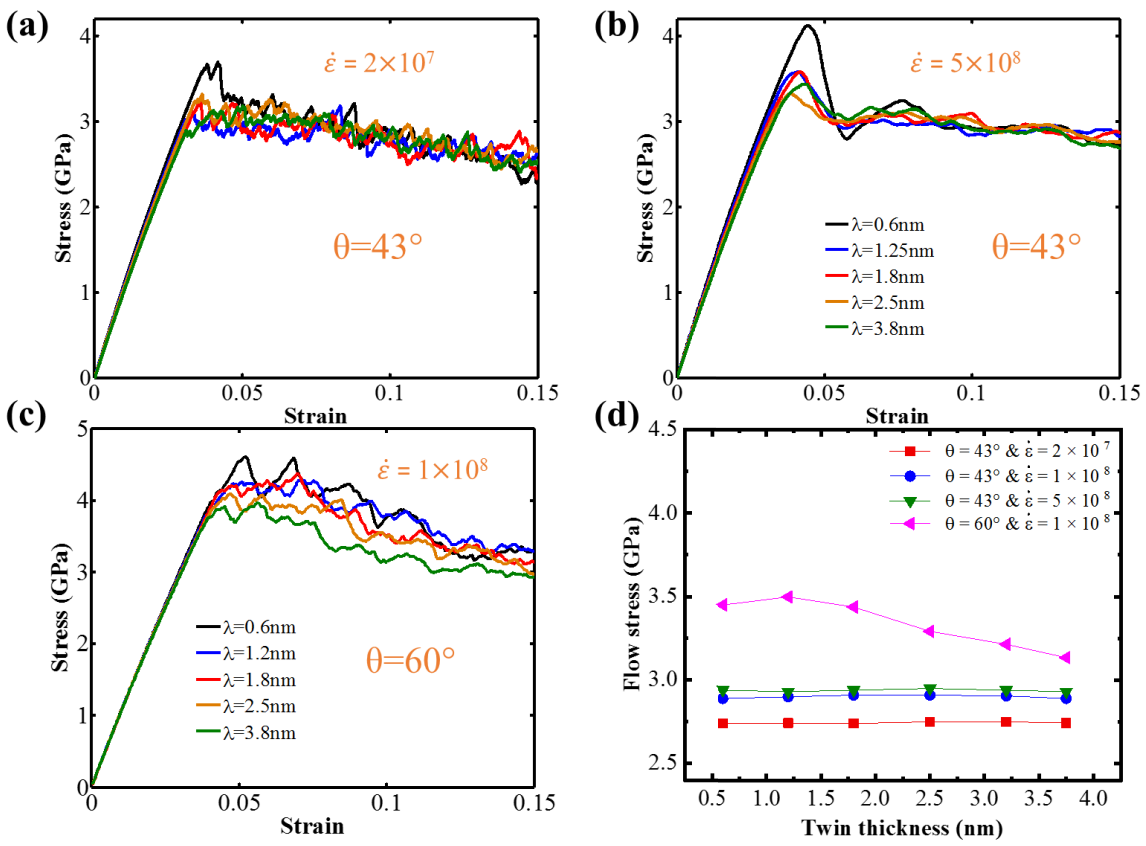

Figure S2. For the case of D = 10 nm, the stress-strain curves for the NT Cu samples for $\theta = 43°$ and (a) $\dot{\varepsilon} = 2\times10^{7}$; (b) $\dot{\varepsilon} = 5\times10^{8}$; and (c) $\theta = 60°$ and $\dot{\varepsilon} = 1\times10^{8}$. (d) Plot of the average flow stress versus the thickness of the twins for the cases shown in (a) - (c).

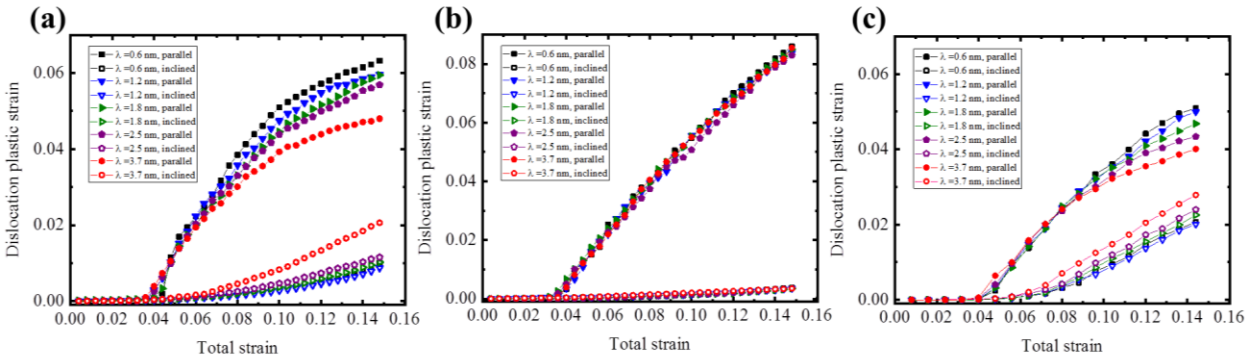

Figure S3. Evolution with strain of the plastic contributions from the TB-parallel and TB-inclined gliding dislocations for NT Cu samples (a) θ = 30°; (b) θ = 43°; (c) θ = 60°. Plastic strain is defined by the atomic shift analysis. For θ = 43°, nearly all cases exhibit the same trend in which the plastic strain contributions from TB-inclined slip is nearly zero and those from parallel slip dominate.

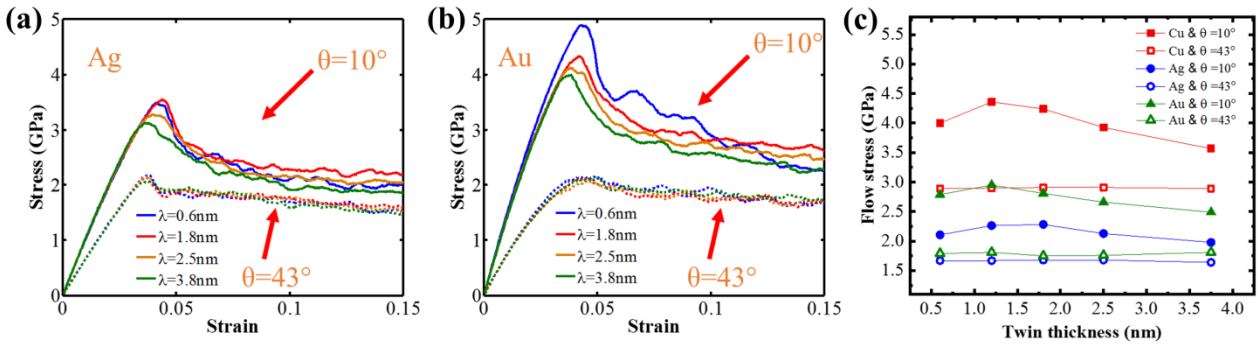

Figure S4. For the case of D = 10 nm, the stress-strain curves for NT samples with (a) Ag with θ = 10° or 43° and (b) Au with θ = 10° or 43°. The solid line represents θ = 10° and the dotted line represents θ = 43°. (c) Plot of the average flow stress versus twin thickness for the cases shown in (a) and (b)

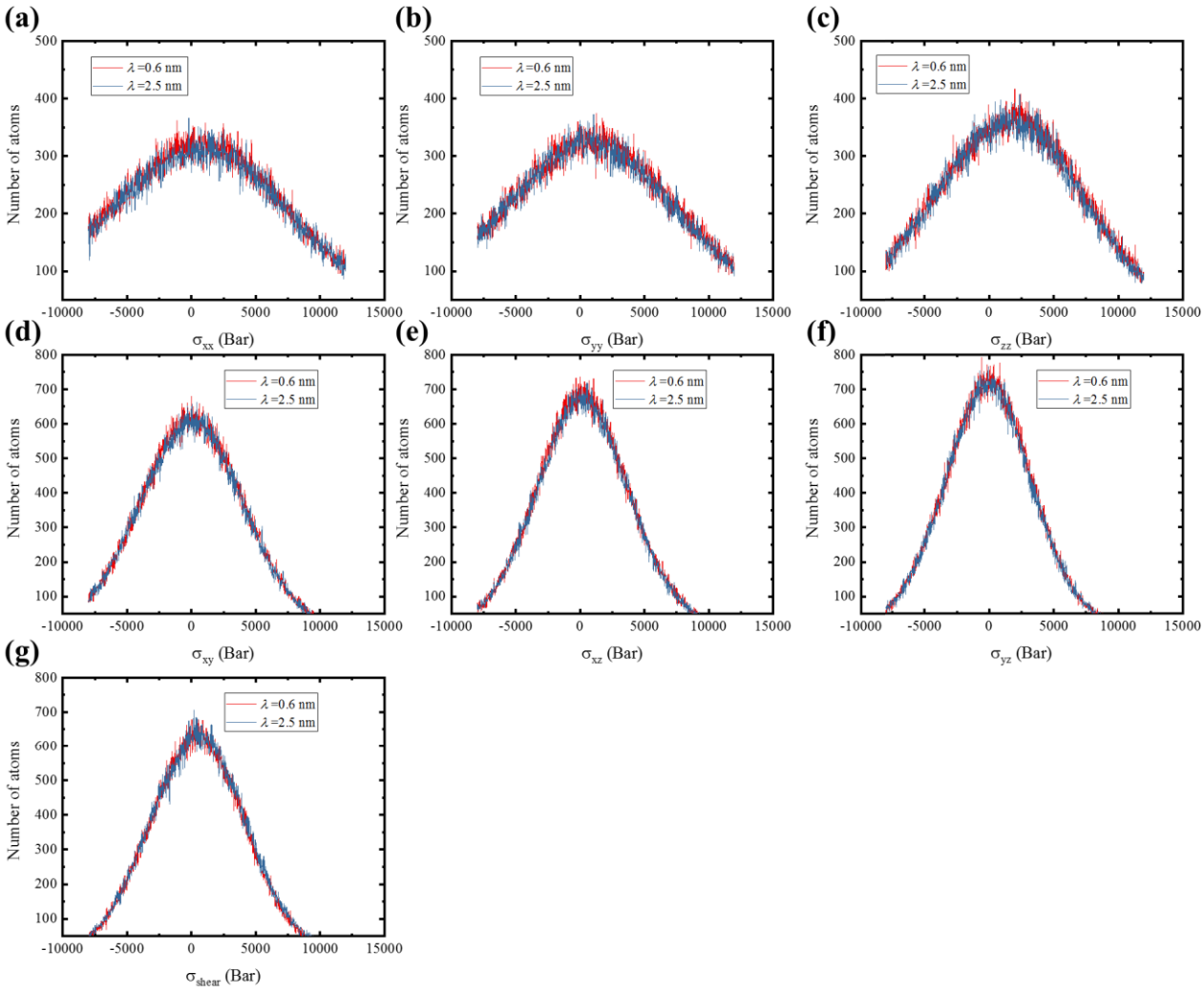

Figure S5. Stress distributions for the atoms at the grain boundaries in the samples with D = 10, θ = 43° and twin boundary spacing λ = 0.6 or 2.5 nm (a) σ_{xx}; (b) σ_{yy}; (c) σ_{zz}; (d) σ_{xy}; (e) σ_{xz}; (f) σ_{yz}; (g) the resolved shear stress, σ_{shear}, on the GB atoms. The analysis was performed at a strain of 2%, which is sufficiently large to identify local stress concentrations but also small enough that stress relaxation by dislocation nucleation would not occur.

Table S1. List of Schmid factors for different slip systems in various tilted twin lamella

Slip system	No tilt	Tilted 10°	Tilted 30°	Tilted 43°
$(111)[11\bar{2}]$	0	0.0855	0.2165	0.2494
$(111)[1\bar{2}1]$	0	0.1710	0.4330	0.4988
$(111)[\bar{2}11]$	0	0.0855	0.2165	0.2494
$(\bar{1}11)[211]$	0.3143	0.2359	0.0477	0.0624
$(\bar{1}11)[12\bar{1}]$	0.1571	0.0859	0.0040	0.0085
$(\bar{1}11)[1\bar{1}2]$	0.1571	0.1501	0.0437	0.0710
$(1\bar{1}1)[121]$	0.3143	0.4283	0.4939	0.4099
$(1\bar{1}1)[21\bar{1}]$	0.1571	0.2142	0.2470	0.2049
$(1\bar{1}1)[\bar{1}12]$	0.1571	0.2142	0.2470	0.2049
$(11\bar{1})[112]$	0.3143	0.2359	0.0477	0.0624
$(11\bar{1})[2\bar{1}1]$	0.1571	0.1501	0.0437	0.0710
$(11\bar{1})[\bar{1}21]$	0.1571	0.0859	0.0040	0.0085

* Assuming the twin boundary parallel to the (111) plane, the first three slip systems are on the slip plane parallel to the twin boundary.

Supplementary Note 1: Simulation results from different strain rates

While studying the effect of strain rate would be insightful, changing the strain rate will not affect the main conclusions of this work. To confirm, the effect of strain rate was tested by simulating the deformation of NT samples with a higher strain rate 5×10^8 and a lower strain rate 2×10^7 than those used in the main simulations discussed here. The stress-strain curves are shown in Figure S2 (a) and (b). For reference, the average flow stress compares with an intermediate strain rate 1×10^8 shown in Figure S2 (d). The twin-thickness-independent phenomenon still prevails for the higher and lower strain rates. The main difference is that the higher strain rate leads to a higher flow stress and the smaller strain rate to a smaller flow stress. This is a consequence of thermally activated dislocation motion [1].

Supplementary Note 2: Simulations of the deformation in nano-twinned Ag and Au

The findings of this work are a consequence of the orientation relationship between the twinned boundaries and preferred slip systems in the FCC structure and thus they should apply to other FCC crystals. To confirm, simulations of nano-twinned Ag and Au were performed for both θ =10º and 43º and the stress-strain curves and average flow stresses are shown in Figure S4. We use the embedded-atom method (EAM) potential for the Ag system developed by Williams et al. [2] and also the EAM potential for the Au system developed by Ackland et al. [3] The twin thickness-independent phenomenon for θ = 43° also exists for these two FCC materials. The average flow stress for all nano-twinned Ag samples are about 1.7 GPa and for all nano-twinned Au samples are about 1.8 GPa. For θ = 10°, the strength increases as λ decreases up to a critical thickness λ_c. As λ decreases below λ_c, the strength decreases, exhibiting an inverse size effect, similar to the nano-twinned Cu samples with θ = 10°.

Supplementary Note 3: Derivative of crystallographic slip model

We estimate the shear strain rates, applying transition state theory for thermally activated slip, based on insight gained on the mechanisms. The dislocation nucleation and gliding for the plastic deformation promoted by the monotonic external loading are considered in our model, while the recovery was ignored, which the same as assuming that there is not barrier for recovery. Specifically, two types of slip modes are revealed, classified by their orientation relationship

with the TBs, and these two would arguably exhibit different rate dependencies. For TB-inclined slip, propagation is limited; the confinement by λ forces the dislocation line to overcome line tension to continuously bow out to move forward. The amount of slip provided by this each inclined slip event is $\frac{b}{D}$. For TB-parallel slip, glide would be limited by the grain size. Consequently, the amount of slip each TB-parallel event induces is $\frac{b}{\lambda}$. The shear strain rate for the inclined slip systems can be expressed as

$$\dot{\gamma}_I = N_I \ \nu_D \ P_I \ \frac{b}{D} \tag{1}$$

where N_I is the number of inclined slip sources per twin lamella, ν_D is the Debye frequency, P_I is the probability that a given inclined source is activated within a unit time, and $\frac{b}{D}$ is the shear strain induced by each inclined slip event. The source number N_I for TB-inclined slip depends on grain size and twin thickness via:

$$N_I = k_I \ \frac{\lambda}{b} \ \frac{D}{b} \tag{2}$$

where k_I is the activation efficiency constant, $\frac{\lambda}{b}$ is the number of sites per inclined slip plane, and $\frac{D}{b}$ is the number of available inclined slip planes.

Assuming that dislocation nucleation is thermally activated we adopt an Arrhenius expression for the probability for source activation:

$$P_I = \exp\left(-\frac{Q-(\tau_{RSS}^I-\tau_I)\,V_I^*}{RT}\right) \tag{3}$$

where the mechanical stress supplied for nucleation is $\tau_{RSS}^I = SF_I\sigma_{App} = \frac{1}{M_I}\,\sigma_{App}$, where σ_{App} is the external applied stress, M_I is the Taylor factors for inclined and parallel slip systems, which are approximately equal to the inverse of their Schmid factors, SF_I. The parameter Q is the activation energy, V_I^* is the activation volume for dislocations on TB-inclined slip planes and $\tau_I = \tau_{CLS}$, which is the critical stress for confined layer slip [4]. Recently, Subedi et al. showed that nanotwinned materials, as well as nanolayered composites, have a macroscopic strength that could be fitted to either the CLS $\ln(\lambda)/\lambda$ dependence or $1/\sqrt{\lambda}$. [5] In our simulation results, we found most inclined dislocations slip within the twin lamella confined by the TBs that is very similar to the boundary condition described in CLS model. In addition, previous experimental

and computational MD simulation works [6, 7] also revealed that the relationship between the tensile strength of columnar twinned Cu and TB thicknesses can be described by CLS model. Thus, we adopted the CLS model to describe the driving stress for TB-inclined slip.

$$\boldsymbol{\tau_{CLS} = M_I \frac{\mu b \sin\varphi}{8\pi\lambda}\left(\frac{4-\nu}{1-\nu}\right)\ln\frac{\alpha\lambda}{b\sin\varphi} - \frac{\gamma}{\lambda} + \frac{\mu b}{l(1-\nu)}} \quad (4)$$

where λ is the twin thickness, μ the shear modulus, ν the Poisson's ratio, φ the angle between slip plane and the layer interface, b the value of the Burgers vector of dislocation, and α is a coefficient representing the extent of the dislocation core.

Combining equations (1)-(4) yields the following equation for the TB-inclined shear strain rate

$$\dot{\gamma}_I = k_I \frac{\lambda}{b}\frac{D}{b}\nu_D \frac{b}{D} exp(-\frac{Q-(\tau^I_{RSS} - \tau_{CLS})V^*_I}{RT})$$

$$= k_I \frac{\lambda}{b}\nu_D exp(-\frac{Q-(\tau^I_{RSS}-\tau_{CLS})V^*_I}{RT}) \quad (5)$$

The shear strain rate for the parallel systems equals to

$$\dot{\gamma}_P = N_P \nu_D P_P \frac{b}{\lambda} \quad (6)$$

where N_P is the number of parallel slip sources per twin lamella, ν_D is the Debye frequency, P_P is the probability that a given parallel source is activated within a unit time, and $\frac{b}{\lambda}$ is the shear strain induced by each TB-parallel slip event.

$$N_P = k_P \frac{\lambda}{b}\frac{D}{b} \quad (7)$$

where k_T is the activation efficiency constant, $\frac{D}{b}$ is the number of sites per parallel slip plane, and $\frac{\lambda}{b}$ is the number of available parallel slip planes.

The activation probability for parallel sources is calculated by

$$P_P = \exp(-\frac{Q-(\tau^P_{RSS}-\tau_P)V^*_P}{RT}) \quad (8)$$

where $\tau^P_{RSS} = SF_P\sigma_{App} = \frac{1}{M_P}\sigma_{App}$ where M_P is the Taylor factors for inclined and parallel slip systems, which are approximately equal to the inverse of their Schmid factors, SF_P. Q is the

activation energy, V_P^* is the activation volume for nucleating dislocations on parallel slip planes, $\tau_P = \tau_{Parallel}$, which is associated with the critical nucleation stress to form partial dislocations [8]

$$\tau_P = \frac{\mu a}{2\sqrt{6} \times \pi \times D} \ln \frac{\sqrt{2}\, D}{a} \tag{9}$$

where a is the lattice constant.

Combining equations (6)-(9) we obtain the following equation for the parallel shear strain rate

$$\dot{\gamma}_T = k_P \frac{\lambda}{b} \frac{D}{b} \frac{b}{\lambda} \nu_D \exp\left(-\frac{Q - (\tau_{RSS}^P - \tau_P) V_P^*}{RT}\right)$$

$$= k_P \frac{D}{b} \nu_D \exp\left(-\frac{Q - (\tau_{RSS}^P - \tau_P) V_P^*}{RT}\right) \tag{10}$$

It is worth mentioning that, the critical threshold values for nucleating dislocations on the inclined and parallel twin boundary slip planes were adopted from references [6, 7] and [8], respectively. The contribution of our MD simulations is to identify the underlying deformation mechanisms in NT metals for developing the slip model to predict the mechanical response and size effect of strength in NT metals respect to the twin boundary orientation.

Supplementary Note 4: Analysis of the stress on GB atoms

In previous studies [9], the inverse size effect in NT Cu was attributed to the nucleation and gliding of dislocations on the TBs in ultrathin twin lamellae. Under this concept, it was rationalized that samples with smaller twin thicknesses carry a higher density of grain-boundary/twin intersections with high stress concentrations, they contain more available sources gliding for dislocations to glide on the TBs (and not in between them). When glide occurs exclusively on the TBs, the twins thicken, triggering the reduction in strength in NT Cu [9]. To quantitatively analyze the effect of λ on the stress concentration on the GB atoms in the case where slip predominantly occurs on parallel slip planes, we calculate the stress distributions for the six stress components and the resolved shear stress (RSS) on the GB atoms for two 43° samples with λ = 0.6 and 2.5 nm, both of which have the same simulation box size (See Figure

S5). The analysis was performed at the strain of 2%, which is large enough to identify the local stress concentrations but also small enough that dislocation nucleation would not occur to relax the stress on the GB atoms. Based on the stress distributions in Figure S5 (a)-(g), these two samples developed similar stress distributions under the applied deformation. The analysis results show that there is no difference on the GB atom stresses between the twin boundary spacing λ = 0.6 and 2.5 nm. Consequently, TB-glide cannot explain the thickness-independent strength for 43º samples observed in current work. One basic assumption in the TB-glide model, is that all dislocations on the parallel slip planes can only nucleate and glide on the twin boundaries [9]. Figures 3(b) and 3(d) from the present simulations find that while some dislocations nucleate and glide on the TBs, a large number of dislocations nucleate and glide on the slip planes, within the twin lamella, and parallel to the TB. Furthermore, those dislocations that glide on the TBs cause the TB to migrate and enlarge the twin. Once the lamella has thickened, dislocations proceed to glide on planes inside them and even TB-inclined slip becomes favorable. Therefore, TB-glide is not predominant and not sustained for most of the deformation and cannot explain the observed inverse size effect.

References

[1] Mecking H, Kocks UF. Kinetics of flow and strain-hardening. Acta Metallurgica 1981;29:1865.

[2] Williams P, Mishin Y, Hamilton J. An embedded-atom potential for the Cu–Ag system. Modelling and Simulation in Materials Science and Engineering 2006;14:817.

[3] Ackland G, Tichy G, Vitek V, Finnis M. Simple N-body potentials for the noble metals and nickel. Philosophical Magazine A 1987;56:735.

[4] Misra A, Hirth J, Hoagland R. Length-scale-dependent deformation mechanisms in incoherent metallic multilayered composites. Acta materialia 2005;53:4817.

[5] Subedi S, Beyerlein IJ, LeSar R, Rollett AD. Strength of nanoscale metallic multilayers. Scripta Materialia 2018;145:132.

[6] You Z, Lu L, Lu K. Tensile behavior of columnar grained Cu with preferentially oriented nanoscale twins. Acta Materialia 2011;59:6927.

[7] Zhou H, Li X, Qu S, Yang W, Gao H. A jogged dislocation governed strengthening mechanism in nanotwinned metals. Nano letters 2014;14:5075.

[8] Zhu Y, Liao X, Srinivasan S, Zhao Y, Baskes M, Zhou F, Lavernia E. Nucleation and growth of deformation twins in nanocrystalline aluminum. Applied physics letters 2004;85:5049.

[9] Li X, Wei Y, Lu L, Lu K, Gao H. Dislocation nucleation governed softening and maximum strength in nano-twinned metals. Nature 2010;464:877.